Stem Cell Reports
Article

ISSCR

OPEN ACCESS

p53 inactivation unmasks histone methylation-independent WDR5 functions that drive self-renewal and differentiation of pluripotent stem cells

Qiang Li,[1] Yuanhao Huang,[2] Jing Xu,[1] Fengbiao Mao,[3] Bo Zhou,[3] Lichao Sun,[3] Brian W. Basinski,[1,3] Michael Aksu,[1] Jie Liu,[2,4] Yali Dou,[3,4,8] and Rajesh C. Rao[1,2,3,4,5,6,7,*]

[1]Department of Ophthalmology & Visual Sciences, W.K. Kellogg Eye Center, University of Michigan, 1000 Wall St., Ann Arbor, MI 48105, USA
[2]Department and Center of Computational Medicine and Bioinformatics, University of Michigan, Ann Arbor, MI, USA
[3]Department of Pathology, University of Michigan, Ann Arbor, MI, USA
[4]Comprehensive Cancer Center, University of Michigan, Ann Arbor, MI, USA
[5]A. Alfred Taubman Medical Research Institute, University of Michigan, Ann Arbor, MI, USA
[6]Center for RNA Biomedicine, University of Michigan, Ann Arbor, MI, USA
[7]Division of Ophthalmology, Surgery Section, VA Ann Arbor Healthsystem, Ann Arbor, MI, USA
[8]Present address: Department of Medicine and Department of Biochemistry and Molecular Medicine, Norris Comprehensive Cancer Center, University of Southern California, Los Angeles, CA, USA
*Correspondence: rajeshr@umich.edu
https://doi.org/10.1016/j.stemcr.2021.10.002

SUMMARY

p53 alterations occur during culture of pluripotent stem cells (PSCs), but the significance of these events on epigenetic control of PSC fate determination remains poorly understood. *Wdr5* deletion in *p53*-null (DKO) mouse ESCs (mESCs) leads to impaired self-renewal, defective retinal neuroectoderm differentiation, and de-repression of germ cell/meiosis (GCM)-specific genes. Re-introduction of a WDR5 mutant with defective H3K4 methylation activity into DKO ESCs restored self-renewal and suppressed GCM gene expression but failed to induce retinal neuroectoderm differentiation. Mechanistically, mutant WDR5 targets chromatin that is largely devoid of H3K4me3 and regulates gene expression in *p53*-null mESCs. Furthermore, MAX and WDR5 co-target lineage-specifying chromatin and regulate chromatin accessibility of GCM-related genes. Importantly, MAX and WDR5 are core subunits of a non-canonical polycomb repressor complex 1 responsible for gene silencing. This function, together with canonical, pro-transcriptional WDR5-dependent MLL complex H3K4 methyltransferase activity, highlight how WDR5 mediates crosstalk between transcription and repression during mESC fate choice.

INTRODUCTION

The interplay of ubiquitous epigenetic factors and transcription factors (TFs) in maintaining pluripotency and directing cell fate is incompletely understood. Pluripotent stem cells (PSCs), such as embryonic stem cells (ESCs) and induced pluripotent stem cells (iPSCs), maintain stemness through self-renewal and harbor the potential to differentiate into any somatic cell type. During PSC cell fate specification, epigenetic histone modifications such as trimethylated lysine 4 on histone H3 (H3K4me3) and H3K27me3 (bivalent chromatin) on embryonic development-related genes undergo dynamic recruitment to coordinate stemness and lineage differentiation (Bernstein et al., 2006). Occupancy of H3K4me3 on the gene promoter typically correlates with gene transcription (Dou et al., 2005, 2006; Li et al., 2012; Rao and Dou, 2015; Wysocka et al., 2005). In contrast, non-canonical H3K4me3 enrichment associated with transcriptional repression has been reported in pre-implantation embryos (Wu et al., 2016). Therefore, whether H3K4me3 recruitment is a cause or consequence of chromatin accessibility and gene transcription remains controversial. H3K4 methylation is a dynamic process controlled by histone methyltransferases and demethylases (Rao and Dou, 2015). H3K4 methyltransferases mainly refer to KMT2 family members (KMT2A-D, F, G), and gene knockout (KO) experiments demonstrated that functional redundancies exist among different KMT2 members (Rao and Dou, 2015). Therefore, a deeper understanding of how H3K4 methylation contributes to gene regulation will provide deep insights into early PSC fate specification.

In mESCs, WDR5 is highly expressed, decreases during differentiation, but remains active in somatic cells (Ang et al., 2011). Expression of WDR5 across cell types is thought to be related to its "epigenetic housekeeping function": H3K4me via the KMT2 (MLL) histone methyltransferase family (Xue et al., 2019). *Wdr5* loss of function leads to lethality in multiple cell types including mESCs (Ang et al., 2011; Li et al., 2020). The majority of reports focus on a "default" function of WDR5 as an activator for gene regulation via its interaction with MLL1 at critical sites (S91 and Y191) at an arginine pocket of WDR5 to modulate H3K4 methylation activity (Dou et al., 2006; Patel et al., 2008b).

Yet, WDR5 represses gene transcription as well and this depends upon interaction with broadly expressed TFs. For instance, WDR5 is also one key component of non-canonical polycomb repressor complex 1 (ncPRC1). Interestingly, three subunits of ncPRC1: PCGF6, and the broadly

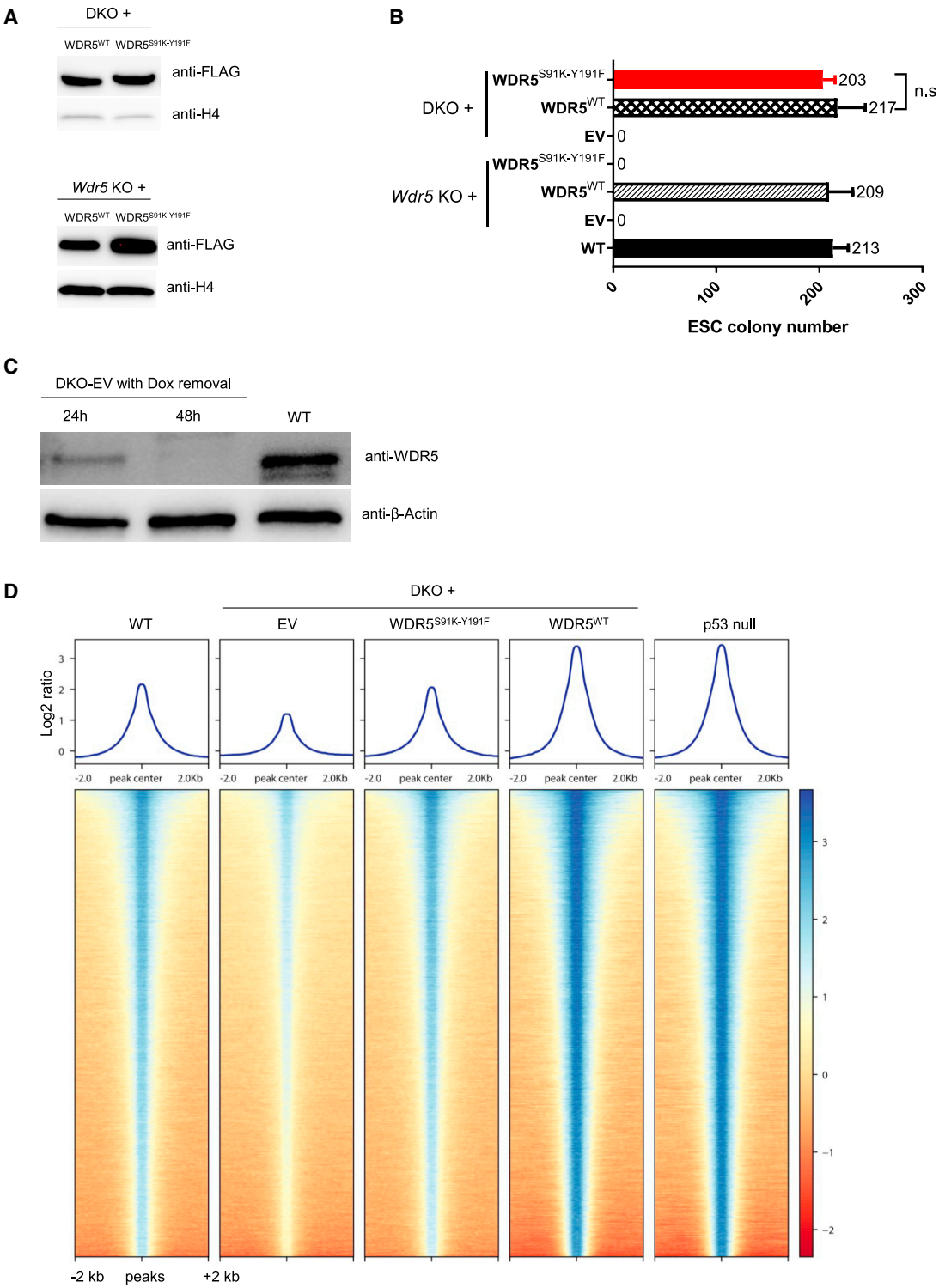

Figure 1. H3K4 methylation-independent function of WDR5 maintains *p53*-null mESC self-renewal

(A) Western blot of FLAG-tagged WDR5^{WT} or WDR5$^{S91K-Y191F}$ in *Wdr5* knockout (KO) and *Wdr5/p53* double knockout (DKO) ESCs with Dox-inducible WDR5^{WT}-HA rescue. Histone H4 was used as loading control.

(B) Clonogenicity of KO, DKO mESCs reconstituted with backbone empty vector (EV), WDR5^{WT} or WDR5$^{S91K-Y191F}$ plasmids. Data presented as mean ± SD (n = 3 independent experiments). n.s., no significant difference.

(legend continued on next page)

expressed TFs MAX and E2F6, have been shown to repress germ cell or meiosis (GCM) gene expression and affect primordial germ cell-like cell (PGCLC) differentiation from mESCs (Endoh et al., 2017; Maeda et al., 2013; Stielow et al., 2018; Suzuki et al., 2016; Velasco et al., 2010).

Another critical TF regulator of WDR5 function in PSC cell fate determination is p53. Like WDR5, p53 is highly expressed in ESCs and decreases during differentiation (Lin et al., 2005). We found that WDR5 interacts with p53 (Li et al., 2020). We identified a repressor function for WDR5, in which its transient inhibition triggers mESC misspecification toward the mesoderm lineage under conditions that normally induce neuroectoderm fate, through a p53-dependent mechanism (Li et al., 2020). p53 is most recognized as a regulator of DNA damage and aberrant *p53* loss-of-function and gain-of-function (GoF) mutations contribute to tumorigenesis (Giaccia and Kastan, 1998; Haupt et al., 1997; Sabapathy et al., 1997). p53 GoF mutants, unlike wild-type (WT) p53, preferentially bind *MLL1* (*KMT2A*), *MLL2* (*KMT2B*), and *MOZ* (*KAT6A*) genes, which result in genome-wide upregulation of H3K4me and H3 acetylation, and enhanced cancer cell proliferation (Zhu et al., 2015). As cancer stem or progenitor cells harbor several hallmarks of PSCs, such as self-renewal and differentiation, it is not surprising that oncogenic *p53* mutations have been also found in multiple mouse and human ESC lines, including those used in ESC-based clinical interventions (Hackett et al., 2018; Merkle et al., 2017). One possible mechanism for accumulation of *p53* mutations in PSC is through selective growth advantage, which is further supported by the observation that *p53* inactivation favors iPSC reprogramming and PGCLC differentiation (Hackett et al., 2018; Marion et al., 2009). However, in PSCs harboring inactivating *p53* mutations, how epigenetic mechanisms modulate self-renewal and cell fate choice remains largely unexplored.

To address these gaps in knowledge related to WDR5-mediated H3K4 chromatin-dependent and/or independent mechanism(s) in *p53*-null mESC self-renewal and neuroectoderm differentiation, here we pursued a series of studies using *Wdr5* and *p53* double KO (DKO) mESC lines carrying doxcycline (Dox)-inducible exogenous WDR5 rescue plasmids. We found that deletion of *Wdr5* in *p53*-null mESCs leads to defective self-renewal, impaired retinal neuroectoderm differentiation and de-repression of GCM-specific gene expression. Reconstitution of DKO mESCs with a mutant form of WDR5 that does not support H3K4 methylation activity revealed that mESC self-renewal and repression of GCM-related expression by WDR5 is H3K4 methylation-independent in *p53*-null mESCs. Furthermore, WDR5-driven, H3K4 methylation-dependent function promotes retinal neuroectoderm differentiation in *p53*-null mESCs. Finally, our study reveals that co-recruitment of MAX and WDR5 to target loci contributes to repression of a subset of genes underlying germ cell development, via changes in chromatin accessibility. Our findings highlight the functional significance of the interaction between the ubiquitous TF and epigenetic regulator, MAX and WDR5, respectively, for mESC fate determination.

RESULTS

WDR5 maintains *p53*-null mouse embryonic stem cell self-renewal in an H3K4 methylation-independent manner

In our recent report, we found that deletion of *p53* in *Wdr5* knockout (DKO) pre-retinal organoids (POs) undergoing lineage specification (day 2 following mESC retinal organoid differentiation) rescued up to 60% of dysregulated genes in *Wdr5* KO POs (Li et al., 2020). To better understand this mechanism, we further examined self-renewal phenotypes in *Wdr5* KO and DKO ESCs carrying with Dox-inducible HA-tagged WT WDR5 (WDR5^{WT}, hereafter referred to as KO or DKO for removal of inducible HA-WDR5^{WT} by Dox washout for 48 h and beyond). Consistent with previous findings (Ang et al., 2011; Gan et al., 2011; Li et al., 2020), *Wdr5* KO ESCs lost self-renewal capacity; this defect was rescued by constitutively expressed FLAG-WDR5^{WT} (Figures 1A, 1B, and S1A).The well-established function of WDR5 is to complex with MLL1 through two critical sites (S91 and Y191) on the MLL1-WDR5 binding interface, which promotes MLL1 histone H3K4 methyltransferase activity (Dou et al., 2006; Patel et al., 2008a, 2008b). A constitutively expressed FLAG-WDR5 compound mutant (i.e., FLAG-WDR5$^{S91K-Y191F}$) failed to rescue *Wdr5* KO mESC clonogenicity, indicating a H3K4 methylation-dependent function for WDR5 on mESC self-renewal, as expected. In contrast, both constitutively expressed FLAG-WDR5^{WT} and FLAG-WDR5$^{S91K-Y191F}$ were able to rescue self-renewal defects in *p53*-null (DKO) mESCs (Figures 1A, 1B, and S1A), indicating an H3K4 methylation-independent role of WDR5 for maintaining *p53*-null mESCs.

To investigate chromatin remodeling secondary to acute loss of WDR5 in *p53*-null ESCs, we performed ATAC

(C) Western blot for detecting residual WDR5 in DKO-EV after Dox (2.0 μg/mL at time 0) washout for 24 or 48 h.
(D) Metaprofiles and heatmaps for ATAC-seq signals centered on peaks closed in DKO-EV mESCs (compared with DKO + WDR5^{WT} controls). n = 2 independent experiments for each group and two independent *p53* KO clones with two independent experiments each were combined for the *p53*-null group.

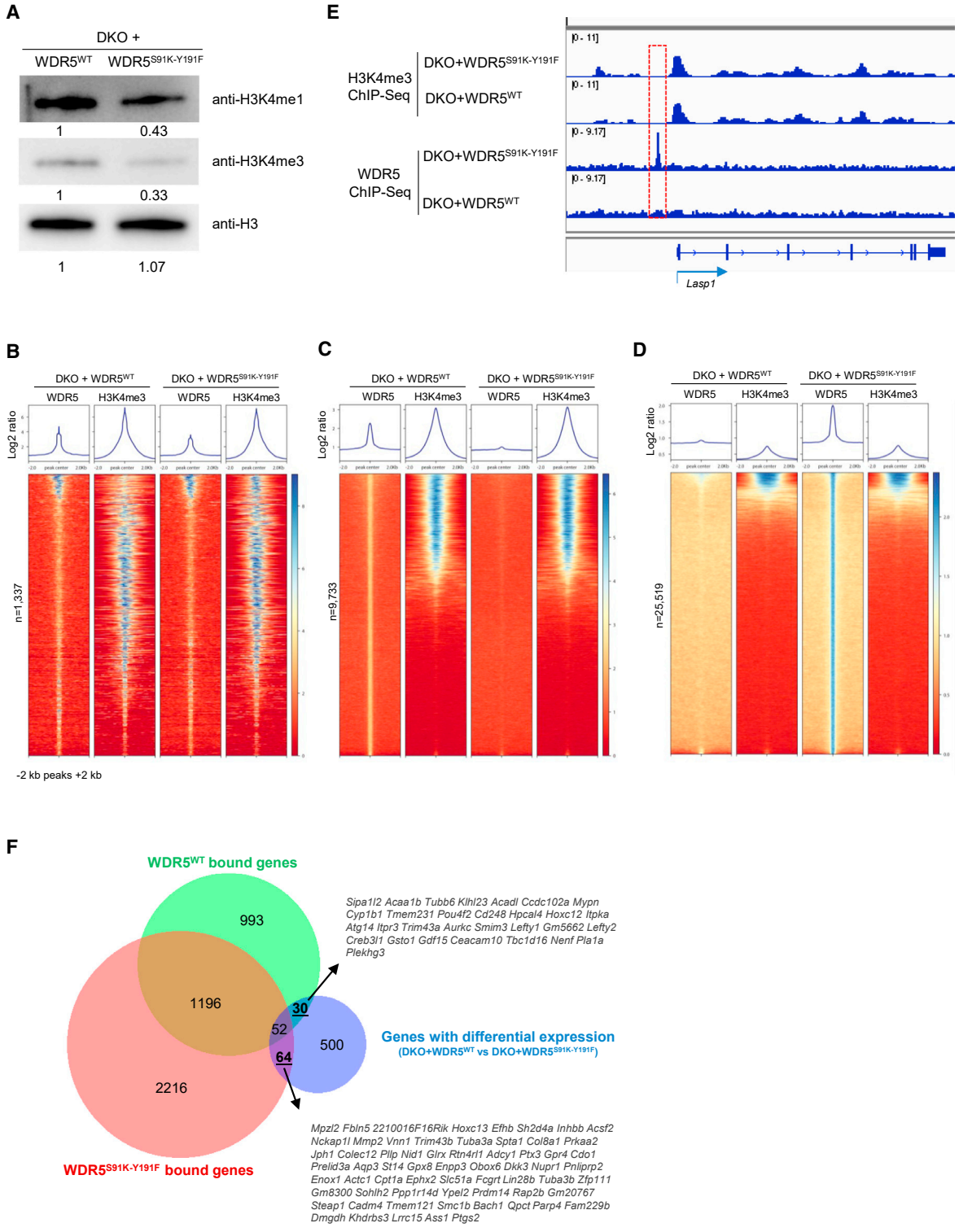

Figure 2. In contrast to WDR5^{WT}, WDR5$^{S91K-Y191F}$ targets chromatin at sites largely devoid of H3K4me3 in *p53*-null mESCs

(A) Western blot to determine global H3K4me1 and H3K4me3 levels in DKO mESCs reconstituted with WDR5^{WT} or WDR5$^{S91K-Y191F}$ plasmids. Relative H3K4me1 or H3K4me3 levels are normalized by loading control histone H3 and setting DKO ESCs reconstituted with WDR5^{WT} as 1 (arbitrary level).

(legend continued on next page)

sequencing (ATAC-seq) in DKO mESCs, by removing Dox for 48 h and in WT parental Rx:GFP mESC controls to assess for differences in chromatin accessibility landscapes (Figure 1C). Interestingly, compared with WT mESC controls, DKO mESCs demonstrated a marked closed chromatin accessibility landscape (20,601 closed peaks representing 9,767 genes and 21 open peaks relative to WT control, respectively; Figure S1B; Table S1). Taking into account that p53 also contributes to chromatin regulation in DKO mESCs, we generated *p53*-null mESCs from a parental WT Rx:GFP ESC line using CRISPR-Cas9 gene editing (Figure S1C) and found that DKO + WDR5^{WT} and *p53*-null ESCs are comparable at the levels of chromatin accessibility (ATAC-seq, Figure 1D) and transcriptomic (RNA sequencing [RNA-seq]; Figure S1D) landscapes. Furthermore, both DKO + WDR5^{WT} and *p53*-null ESCs demonstrated more open chromatin accessibility compared with parental WT Rx:GFP mESCs (column 4 or 5 versus column 1 in Figure 1D), which is consistent with previous findings that p53 binds within structurally inaccessible regions of chromatin (Sammons et al., 2015). Re-introduction of WDR5$^{S91K-Y191F}$ partially reversed closed chromatin accessibility found in DKO ESCs, but this chromatin accessibility "rescue" was to a lesser extent than that of WDR5^{WT} mESCs (Figures 1D and S1E). Together, we conclude that *p53* inactivation in *Wdr5* KO mESCs unmasks an H3K4 methylation-independent function for WDR5 in self-renewal of *p53*-null mESCs.

WDR5$^{S91K-Y191F}$ rewires the WDR5-chromatin interaction to exert H3K4me3-independent function in *p53*-null mouse embryonic stem cells

As exogenous expression of WDR5$^{S91K-Y191F}$ has been widely used to interrogate H3K4 methylation-independent chromatin function of WDR5 (Dou et al., 2006; Kulkarni et al., 2018; Kulkarni and Khokha, 2018; Patel et al., 2008b), we next asked how WDR5$^{S91K-Y191F}$ directly regulates target gene expression in *p53*-null mESCs. Expression of WDR5$^{S91K-Y191F}$ reduced global histone H3K4me3 levels compared with expression of WDR5^{WT} in both DKO mESCs and POs (Figures 2A and S2A), which is consistent with previous findings (Dou et al., 2006). To further investigate these observations at higher resolution, chromatin immunoprecipitation followed by sequencing (ChIP-seq) using antibodies against H3K4me3 and WDR5 was conducted. Among all WDR5 ChIP-seq peaks (n = 36,589), only 3.6% (1,337/36,589) of targets were shared by both WDR5^{WT} and WDR5$^{S91K-Y191F}$ (Figure 2B). Interestingly, shared WDR5^{WT} and WDR5$^{S91K-Y191F}$ peaks were largely co-occupied by H3K4me3 signals (Figure 2B). Within this subset of overlapping peaks at which WDR5^{WT}, WDR5$^{S91K-Y191F}$, and H3K4me3 all bound, loci encoding ribosomal biogenesis genes *Rpl5* and *Rpl11* were found (Figure S2B). These data suggest that WDR5 association with particular loci is H3K4 H3K4 methylation-independent, since both WDR5^{WT} and WDR5$^{S91K-Y191F}$ target H3K4me3-decorated chromatin (Figure S2B). Among differential peaks analyzed, 26.6% (9,733/36,589) were WDR5^{WT} specific (Figure 2C) and 69.7% (25,519/36,589) were WDR5$^{S91K-Y191F}$ specific (Figure 2D). Only ~50% of loci with exclusive WDR5^{WT} occupancy exhibited H3K4me3 modification (Figure 2C), indicating H3K4me3-dependent (Figure S2C) and -independent (Figure S2D) functions of WDR5^{WT} in DKO mESCs. In contrast, most gene loci with exclusive WDR5$^{S91K-Y191F}$ enrichment were without H3K4me3 modifications in DKO mESCs (Figures 2D and 2E). Based on differential WDR5^{WT} versus WDR5$^{S91K-Y191F}$ bound peaks across the genome, and the fact the H3K4me3 was not present at most WDR5$^{S91K-Y191F}$ bound peaks, we concluded that WDR5$^{S91K-Y191F}$ rewires the WDR5-chromatin interaction to exert H3K4me3-independent function in DKO mESCs. Finally, WDR5 ChIP-seq data (Figures 2C and 2D) was integrated with RNA-seq data (Table S2) to identify changes in target gene transcription at loci bound by WDR5^{WT} or WDR5$^{S91K-Y191F}$ in *p53*-null mESCs (i.e., direct target genes). *Lefty1* and *Lefty2*, among the 30 WDR5^{WT} direct target genes, have been reported to balance ESC self-renewal and differentiation (Kim et al., 2014a) (Figure 2F). *Prdm14*, *Lin28b*, and *Bach1*, among the 64 WDR5$^{S91K-Y191F}$ direct target genes, regulate PSC reprogramming and chromatin maintenance (Nady et al., 2015; Niu et al., 2021; Shyh-Chang and Daley, 2013) (Figure 2F). Collectively, these data indicate that, by targeting distinct loci compared with WDR5^{WT}, which are largely devoid of H3K4me3, WDR5$^{S91K-Y191F}$ rewires the WDR5-chromatin interaction in an H3K4 methylation-independent manner and regulates target gene expression in *p53*-null mESCs.

(B) Metaprofiles and heatmaps of ChIP-seq signals centered on common peaks bound by both WDR5^{WT} and WDR5$^{S91K-Y191F}$ (n = 1,337).
(C) Metaprofiles and heatmaps of ChIP-seq signals centered on WDR5^{WT}, but not WDR5$^{S91K-Y191F}$, bound peaks (n = 9,733).
(D) Metaprofiles and heatmaps of ChIP-seq signals centered on WDR5$^{S91K-Y191F}$, but not WDR5^{WT}, bound peaks (n = 25,519).
(E) Representative track views of WDR5$^{S91K-Y191F}$, but not WDR5^{WT}, bound peaks, and corresponding H3K4m3 signals as determined by WDR5 or H3K4me3 ChIP-seq, respectively.
(F) Venn diagram integration WDR5^{WT} or WDR5$^{S91K-Y191F}$ bound genes (determined by ChIP-seq) with differentially expressed genes between DKO + WDR5^{WT} versus DKO + WDR5$^{S91K-Y191F}$ (determined by RNA-seq). WDR5^{WT} (n = 30) or WDR5$^{S91K-Y191F}$ (n = 64) direct target genes in DKO ESCs are presented individually.

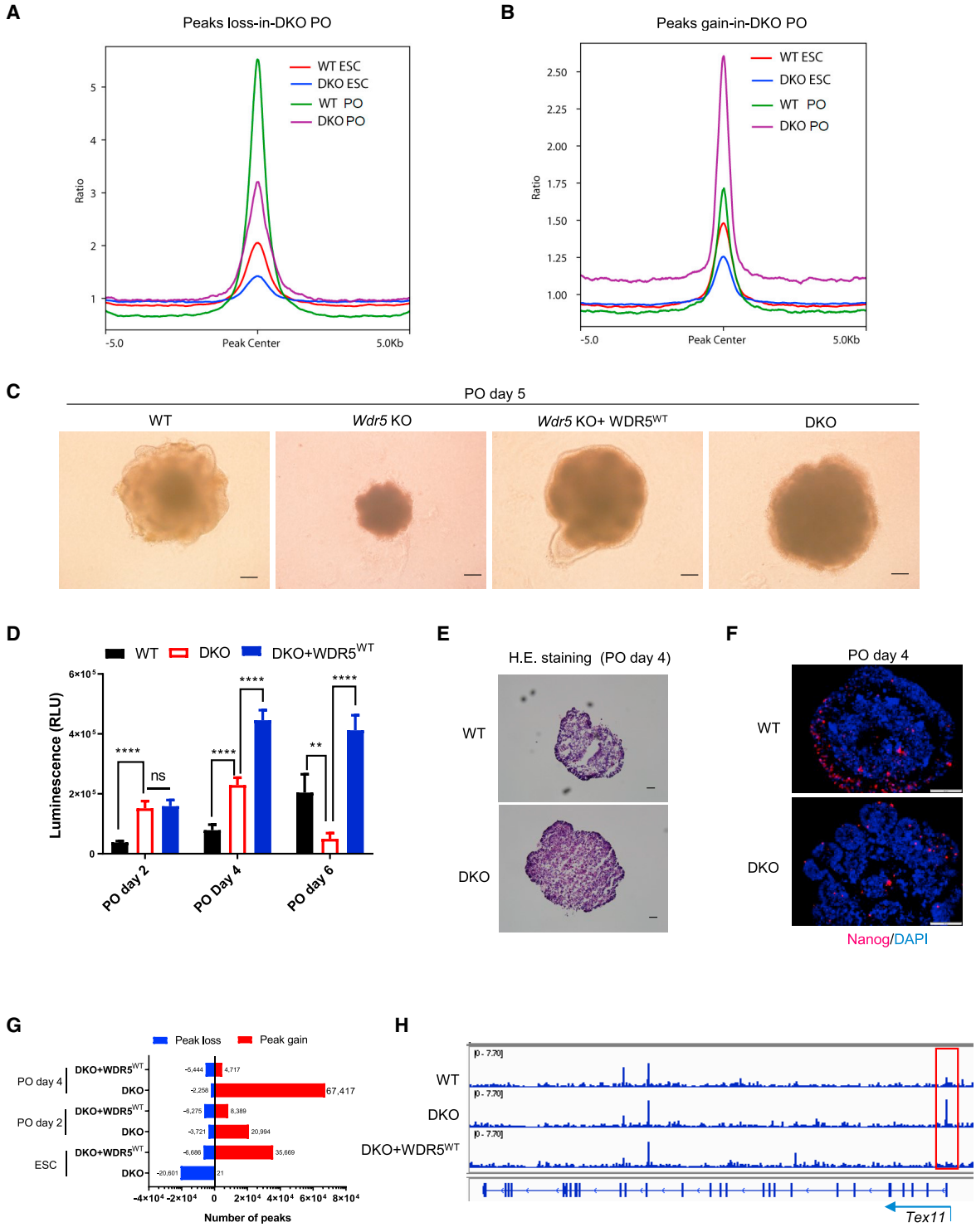

Figure 3. Deletion of *Wdr5* and p53 in ESCs and POs leads to distinct chromatin accessibility dynamics

(A and B) Metaprofiles of mESC and PO ATAC-seq signals centered on peaks lost (A) or gained (B) in POs upon deletion of *Wdr5* and *p53* for 48 h (DKO), and relative to DKO POs.

(C) Morphology of day 5 WT, *Wdr5* KO, and DKO POs with or without $WDR5^{WT}$ rescue. Scale bars, 50 μm.

(legend continued on next page)

Deletion of *Wdr5* and *p53* leads to marked increase of chromatin accessibility during DKO mouse embryonic stem cell-to-pre-organoid differentiation

Having unmasked non-canonical, H3K4 methylation-independent roles for WDR5 in chromatin accessibility and self-renewal of *p53*-null mESCs (Figures 1, 2, S1, and S2), we next explored potential functions for WDR5 that control chromatin accessibility and cell fate specification during DKO mESC differentiation. To this end, we used a serum-free embryoid body with quick aggregation protocol (SFEBq) to generate 3D retinal neuroectodermal organoids from mESCs, as described previously (Eiraku and Sasai, 2011; Li et al., 2020). To determine whether WDR5- and p53-dependent chromatin accessibility in POs were state-specific or pre-existing in mESCs, we compared ATAC-seq profiles of WT versus DKO mESC and PO states. To this end, we withdrew Dox treatment, resulting in removal of Dox-inducible WDR5WT-HA^{WT} for 48 h, and then analyzed mESCs and day 2 POs by ATAC-seq. For peaks with reduced chromatin accessibility in DKO POs relative to WT POs ("peaks loss-in-DKO PO"), DKO mESC ATAC-seq signals were also reduced relative to that of in WT ESCs (Figure 3A). On the other hand, peaks with increased chromatin accessibility in DKO POs relative to WT POs ("peaks gain-in-DKO PO") showed low signal intensities in mESCs in general and were differentially less accessible in DKO mESCs versus those of WT mESCs (Figure 3B). Distinct chromatin accessibility patterns in WT versus DKO at mESC and PO stages suggested that WDR5 and p53 regulate chromatin accessibility through context-specific manner, which is dependent on differentiation stage (undifferentiated mESCs or differentiating POs). Unlike WT mESC-derived POs, we found that DKO POs did not maintain viability beyond 5 days of SFEBq differentiation (Figure 3C). Indeed, cell proliferation defects were observed at day 6 (Figure 3D). However, we were able to reproducibly recover proliferative day 4 DKO POs, which underwent exit from pluripotency, as signified by reduced NANOG expression (Figures 3E and 3F). Thus, we performed ATAC-seq on DKO PO cells at this time point. Strikingly, day 4 DKO POs showed increased chromatin accessibility relative to day 4 WT POs (Figures 3G, S3A, and S3B). To further exclude that marked open chromatin accessibility observed in DKO POs was not due to artifacts or off-target effects, Dox-inducible WDR5^{WT}-HA was added back to DKO POs at 12 h post differentiation. Of peaks in DKO POs that became accessible (closed-to-open peaks) due to deletion of *Wdr5*, ~60% and ~90% closed at day 2 and 4 POs, respectively, with WDR5WT-HA^{WT} rescue (Figures 3G and 3H). We conclude that DKO POs display open chromatin accessibility specific to differentiation stages (e.g., day 2 and 4), while in mESCs with *Wdr5* and *p53* deletion, regions with closed chromatin accessibility are predetermined at the pluripotent stage.

Wdr5 and *p53* deletions trigger mESC misspecification during neuroectoderm differentiation and ectopic de-repression of germ cell- and meiosis-specific genes

To further understand the implications of WDR5-dependent changes in the chromatin accessibility landscape on lineage specification, we performed RNA-seq to identify differentially expressed genes in WT versus DKO POs at the day 4 time point. When we compared differentially expressed genes between WT and POs from two independently derived DKO mESCs (DKO-A and DKO-B), we found a high confidence set of 1,315 downregulated genes (Figure 4A; Table S3). Upregulated or downregulated mRNA expression determined by RNA-seq correlates to some extent, but not entirely, to open or closed chromatin accessibility states in day 4 WT and DKO POs (Figure S3C). Gene ontology (GO) analysis showed that pathways related to retinal neuroectoderm differentiation including eye development and neurogenesis were affected in DKO POs (Figures 4B and S3D). Indeed, in contrast to our observation of retinal neuroectoderm-specific Rx:GFP (+) cell induction in WT retinal neuroectodermal organoids after 6 days of differentiation, we observed defective Rx:GFP (+) cell induction in DKO organoids (see Figures 5C and 5D). Interestingly, for 680 upregulated genes observed in day 4 DKO POs relative to WT POs (Figure 4C; Table S3), GO analysis indicated that pathways related to GCM and chromosome segregation were over-represented (Figure 4D). Heatmaps demonstrated that 35 representative GCM-related genes, including *Ddx4* (*Vasa*), *Dazl*, *Dppa3*, *Stag3*, *Smc1β*, and *Tex11* were significantly upregulated in DKO POs (Figure 4E), consistent with open chromatin accessibility in promoters of 17 GCM-specific genes such as *Tex11* observed in DKO POs (Figure 3H). In summary,

(D) Cell proliferation of day 2, 4, and 6 WT and DKO POs with or without WDR5^{WT} rescue. n = 4–6 independent experiments for each time point. **p $\leq$ 0.01 compared with WT controls. ****p $\leq$ 0.0001 compared with WT controls.

(E) H&E staining of day 4 WT and DKO POs. Scale bars, 50 μm.

(F) Immunostaining of Nanog in day 4 WT and DKO POs. DAPI is counter stained for nuclear DNA. Scale bars, 100 μm.

(G) Number of ATAC-seq peaks lost or gained in DKO mESCs, day 2 and 4 POs with or without WDR5^{WT} rescue. DKO + WDR5^{WT} mESCs or POs at the respective time points are set as controls.

(H) Representative track views of chromatin accessibility in *Tex11* gene promoter in WT and DKO POs with or without WDR5^{WT} rescue at day 4.

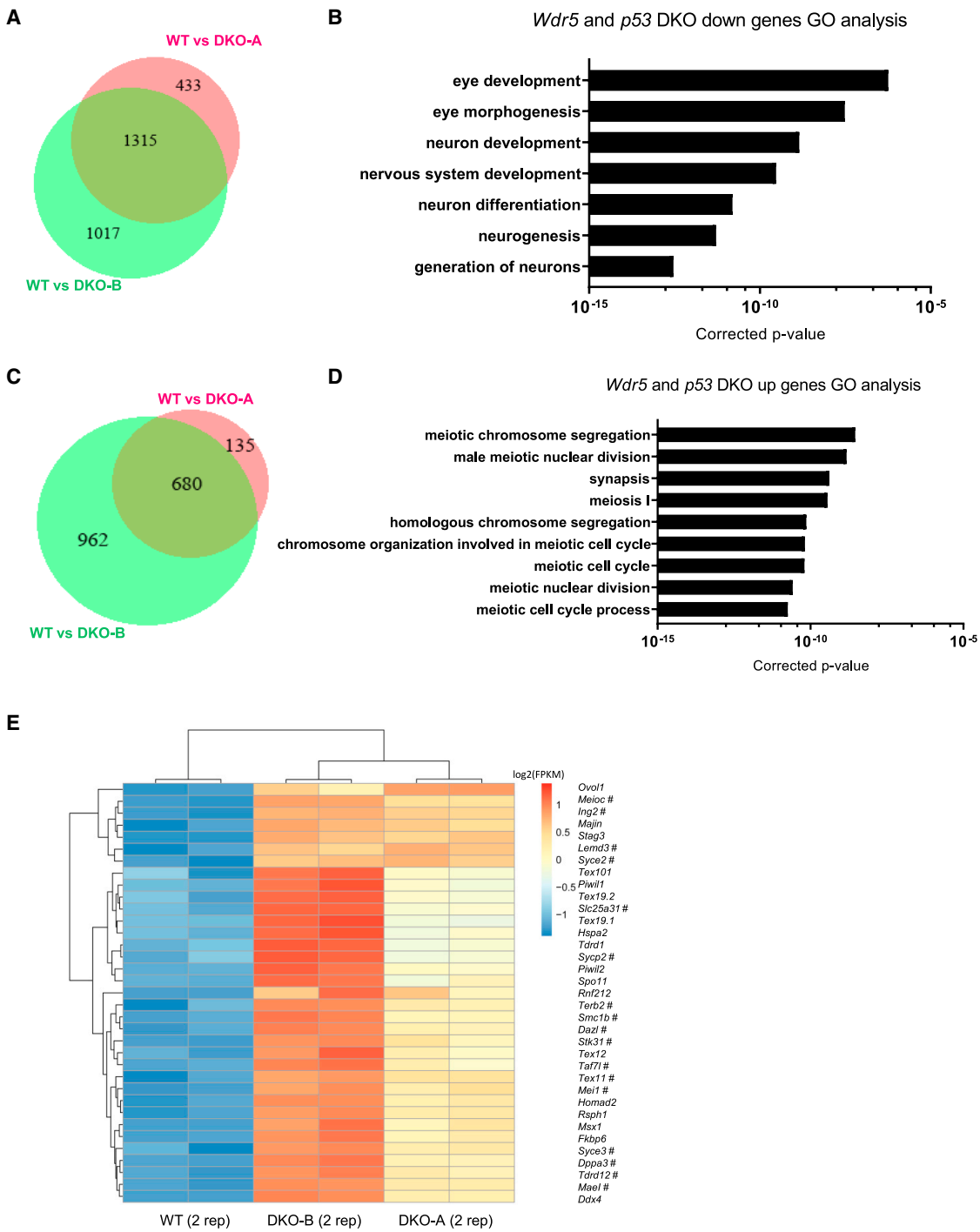

Figure 4. *Wdr5* deletion in *p53*-null POs leads to impaired retinal neuroectoderm differentiation and de-repression of germ cell/meiosis-related genes

(A and B) Venn diagram (A) and gene ontology analysis (B) of downregulated genes overlapped in two independent DKO mESC lines (DKO-A and DKO-B).

(C and D) Venn diagram (C) and gene ontology analysis (D) of overlapping upregulated genes in two independent DKO mESC lines.

(E) Heatmaps for differential expression of GCM-related genes in WT and two independent DKO mESC lines. Gene labeled with # indicated open ATAC-seq chromatin accessibility in respective gene promoters.

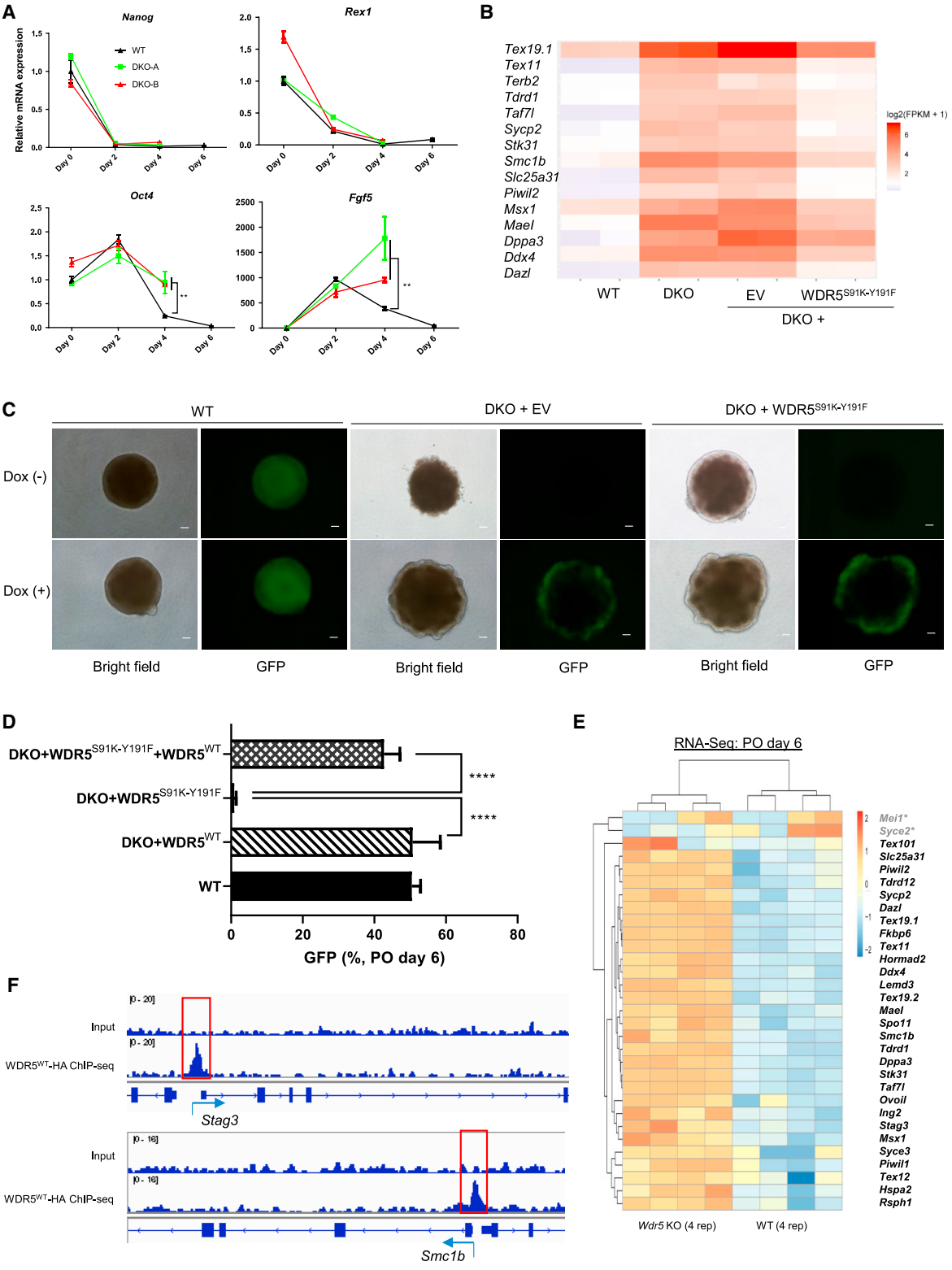

(legend on next page)

transcriptome analysis indicates that deletion of *Wdr5* and *p53* leads to impaired retinal ectoderm differentiation and upregulation of GCM-related genes.

Differential requirement for WDR5-mediated H3K4 methylation in regulating expression of retinal neuroectoderm- versus germ cell and meiosis-related genes

Induction of GCM-specific genes is required for mESC-to-PGCLC differentiation. This cell fate transition occurs through an epiblast-like cell (EpiLC) transition state (Hayashi et al., 2011). Based on the open chromatin accessibility and upregulation of GCM-related genes in day 4 DKO POs, we performed time course differentiation to analyze dynamic gene markers during this mESC-to-EpiLC-to-PGCLC transition phase. We observed that differentiation-induced silencing of mESC stemness genes *Nanog* and *Rex1* was similar in WT and DKO cells (Figure 5A), indicating proper exit from pluripotency. EpiLCs express OCT4 and FGF5 (Liu et al., 2015). *Oct4* silencing was observed in day 4 WT POs while DKO POs showed delayed silencing of *Oct4* gene. DKO POs exhibited significant higher induction of *Fgf5* than WT control at day 4 POs (Figure 5A). Confocal microscopy of day 4 whole POs with 3D re-construction showed that WT (Video S1) and DKO POs (Video S2) had similar distribution of $OCT4^{+}FGF5^{+}$ double-positive EpiLCs (29% versus 36.3%, respectively). Although day 4 DKO POs had upregulation of *Dppa3* (*Stella*) and GCM-related genes, other bone fide PGCLC markers *Prdm1*, *Prdm14*, and *Tfap2c* were not present (Figures 4E and S3E). Further flow cytometric analysis suggested that there were no $SSEA1^{+}/CD61^{+}$ PGCLCs detected in both WT and DKO POs (data not shown). These data suggested that day 4 DKO POs may represent an intermediate differentiation state between EpiLCs and PGCLCs (Hayashi et al., 2011).

We next asked whether H3K4 methylation-dependent or -independent chromatin regulation by WDR5 contributes to transcriptional output in day 4 DKO POs. Re-introduction of $WDR5^{S91K-Y191F}$ was able to partially rescue 31 downregulated genes and 48 upregulated genes in day 4 DKO POs (Figures S3F and S3G), respectively. Of note, ~40% (15/35) of GCM-related genes upregulated in day 4 DKO POs were repressed by $WDR5^{S91K-Y191F}$ (Figure 5B). In contrast, of 154 genes responsible for neurogenesis downregulated in DKO POs (Figure S3D), only 1 gene (*Ror2*) was rescued by $WDR5^{S91K-Y191F}$ in day 4 DKO POs. Thus, these data further supported that impaired retinal neuroectoderm differentiation in DKO by $WDR5^{S91K-191F}$ is not the consequence of a dominant-negative effect, as this defect can be rescued by co-expression of Dox-inducible $WDR5^{WT}$-HA (Figures 5C and 5D).

To determine whether WDR5 alone is sufficient to repress GCM genes, we re-analyzed day 2 PO RNA-seq data from our previous report and found that GCM-related genes, including *Dppa3*, *Stag3*, *Smc1β*, *Syce3*, *Dazl*, *Rhox5*, *Spo11*, *Stk31*, *Tex101*, *Tex13c2*, *Tex19.2*, and *Tex21* were upregulated in day 2 *Wdr5* KO POs (Li et al., 2020). The majority of GCM-specific genes upregulated in day 4 DKO POs (Figure 4E) were also induced in day 6 *Wdr5* KO POs (Figure 5E). Derepression of GCM genes in day 2 and day 6 *Wdr5* KO supported that WDR5 plays essential roles for GCM-related gene regulation. Integration of $WDR5WT\text{-}HA^{WT}$ ChIP-seq and RNA-seq data from day 6 POs in our previous report was performed and of 29 GCM-specific genes repressed by WDR5 (Figure 5E), we identified four WDR5 direct target genes: *Stag3*, *Smc1β*, *Ing2*, and *Dazl* (Figure 5F). Together with our *Wdr5* KO and DKO PO findings (Figure 3E), we conclude that: (1) a subset of GCM-specific genes are direct WDR5 targets and (2) WDR5-mediated repression of a subset of GCM genes is independent of H3K4 methylation activity. In contrast, in identical differentiation conditions, WDR5-driven activation of retinal neuroectoderm lineage-specifying gene is H3K4 methylation-dependent (Figure 5C).

Interaction of MAX and WDR5 contributes to chromatin accessibility during early *Wdr5* KO pre-organoid differentiation

WDR5 is a subunit of the ncPRC1 complex and at least three of the ncPRC1 components repress GCM-related

Figure 5. Differential requirement for WDR5-mediated H3K4 methylation in regulation of retinal neuroectoderm and germ cell/meiosis-related gene expression in DKO POs

(A) Time course qRT-PCR analysis of genes for mESC pluripotency exit and ESC-to-EpiLC transition in WT and DKO mESCs or POs. DKO-A and DKO-B indicates two independent DKO mESC lines. n = 3 independent experiments. $^{**}p \leq 0.01$ compared with WT controls.

(B) RNA-seq analysis shows rescue effect of $WDR5^{S91K-Y191F}$ on "re-repression" of germ cell/meiosis-related genes at day 4 DKO POs. EV, empty vector. n = 2 independent experiments.

(C) Rx:GFP reporter tracks for retinal neuroectoderm organoid differentiation at day 6 WT or DKO POs rescued with backbone EV or $WDR5^{S91K-Y191F}$ plasmids. Dox, doxycycline-inducible HA-$WDR5^{WT}$ rescue. Scale bars, 50 μm.

(D) Quantification of day 6 Rx:GFP (+) cells using flow cytometry on DKO POs rescued with $WDR5^{WT}$ and/or $WDR5^{S91K-Y191F}$. n = 2 independent experiments (eight individual POs for each replicate). $^{****}p \leq 0.0001$ compared with the DKO + $WDR5^{S91K-Y191F}$ group.

(E) Heatmaps of meiosis-related gene expression in day 6 WT and *Wdr5* KO POs. Two genes (*Mei1* and *Syce2*) had no differential expression are labeled with an asterisk (*).

(F) Representative track views of HA-$WDR5^{WT}$ binding peaks at *Stag3* and *Smc1β* gene promoters determined by ChIP-seq on day 6 POs.

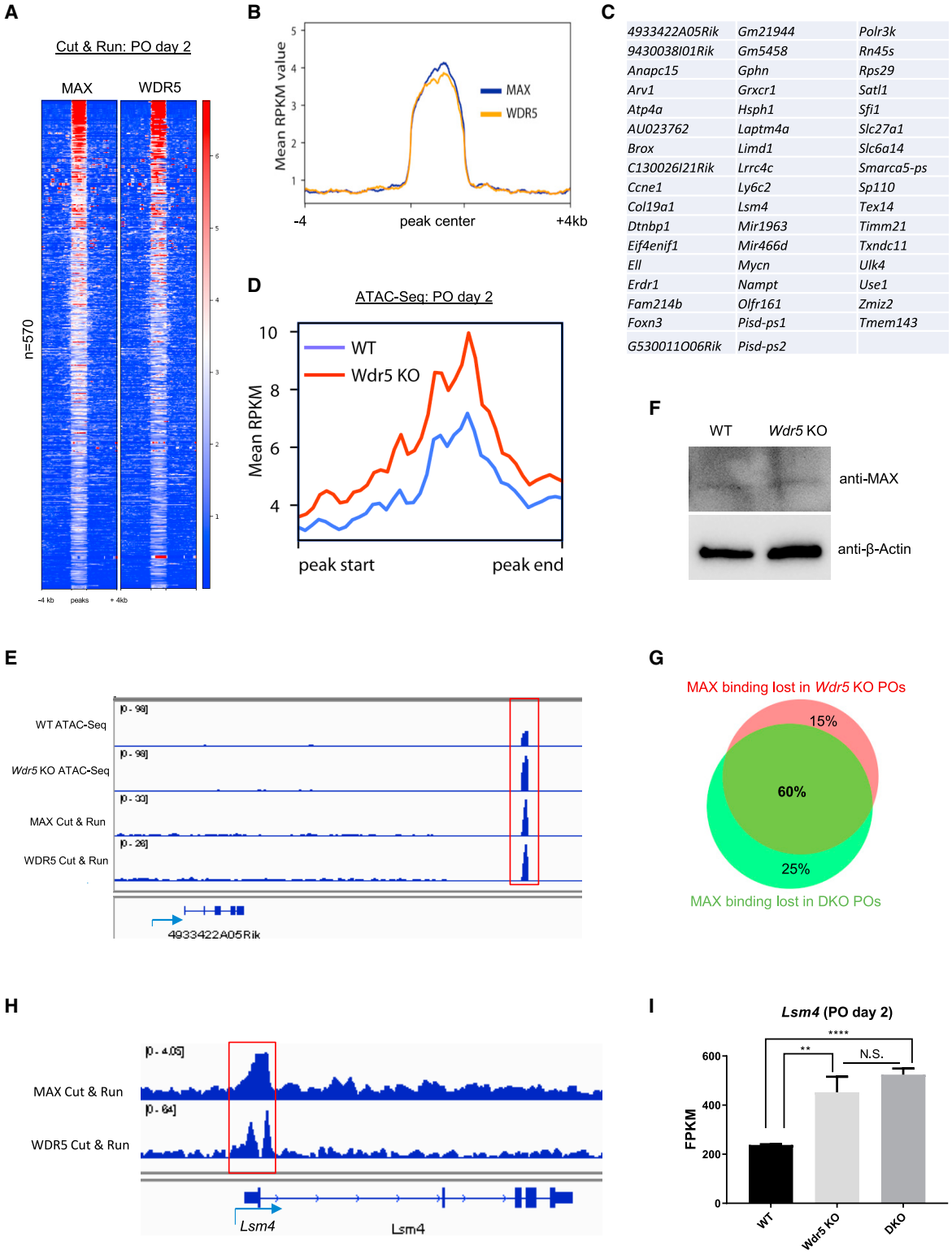

Figure 6. MAX and WDR5 bind to common gene targets during mESC-to-retinal neuroectoderm differentiation

(A and B) Heatmaps (A) and metaprofiles (B) of MAX and WDR5 CUT&RUN signals centered on MAX bound peaks in day 2 POs.

(C and D) List (C) and metaprofiles (D) for MAX and WDR5 co-bound genes which displayed differential chromatin accessibility upon *Wdr5* deletion at day 2 POs. All genes except *Tmem143* had increased and open chromatin accessibility.

(legend continued on next page)

gene expression in mESCs: MAX, PCGF6, and E2F6 (Endoh et al., 2017; Maeda et al., 2013; Stielow et al., 2018; Suzuki et al., 2016). Since *Wdr5* deletion in mESCs and POs phenocopied *Max*-null mESCs and EBs (i.e., loss of self-renewal and viability, and de-repression of GCM-related genes), we hypothesized that interaction of MAX and WDR5 mediates GCM-specific gene repression during early retinogenesis (Maeda et al., 2013; Suzuki et al., 2016). To this end, we performed cleavage under targets & release using nuclease (CUT&RUN) on day 2 POs using a validated MAX antibody (Blazevits et al., 2020; Meers et al., 2019a, 2019b). Heatmaps and metaprofiles from CUT&RUN showed that MAX-bound chromatin targets largely overlapped with those of WDR5 bound (Figures 6A and 6B), consistent with a previous report that MAX interacts with WDR5 (Dou et al., 2005) and was further confirmed in our experiments (data not shown). Integration of MAX/WDR5 co-bound genes in day 2 POs (by CUT&RUN) with ATAC-seq of day 2 WT versus *Wdr5* KO POs revealed that *Wdr5* deletion led to open chromatin accessibility in 49 out of 50 genes bound by both MAX and WDR5 (Figures 6C and 6D). Of those genes, *4933422A05Rik* (Figure 6E) and *Tex14* are selectively expressed in the testis, which is largely comprised of germ cells (Greenbaum et al., 2007; Yue et al., 2014). *Ccne1* is an important regulator for male meiosis (Martinerie et al., 2014). *Lsm4* and *Ell* are downstream targets of master regulator DAZL, and regulate germ cell differentiation and survival (Zagore et al., 2018). Acute deletion of *Wdr5* did not affect general MAX protein level (Figure 6F). MAX recruitment was diminished at a similar set of gene targets (60% overlapping) in both day 2 *Wdr5* KO and DKO POs (Figure 6G). Importantly, reduction of both MAX and WDR5 enrichment to 5′ UTR of *Lsm4* gene at day 2 *Wdr5* KO and DKO POs correlated with upregulated *Lsm4* mRNA expression (Figures 6H and 6I). Thus, MAX and WDR5 co-target a common region of the *Lsm4* gene to repress or limit its expression in day 2 POs. Taken together, our data indicate that a MAX-WDR5 interaction regulates GCM-related chromatin accessibility and gene expression during early retinal neuroectoderm differentiation. Our findings reveal an H3K4 methylation-independent function of WDR5 in gene regulation and cell fate choice during mESC self-renewal and early differentiation.

DISCUSSION

As a core subunit of MLL1 histone methyltransferase complex, WDR5 promotes H3K4 methylation at actively expressed genes and is required for growth for a variety of cancers (Kim et al., 2014b; Rao and Dou, 2015). Thus, WDR5 has attracted intense biopharmaceutical interest as a pharmacologic target (Kim et al., 2014b; Rao and Dou, 2015; Schapira et al., 2017) (https://facit.ca/news/facit-and-triphase-accelerator-announce-new-partnership-celgene-first-class-wdr5-leukemia). Moreover, given the essential role of WDR5 in mESC self-renewal and differentiation and the use of human ESC-derived tissues for therapies, a deeper understanding of the relationship between WDR5 and p53 is important. This is because dominant-negative *TP53* mutations have been detected in human ESC lines (H9 line) later used in ESC-derived cell therapy human trials and *TP53* mutations exist in approximately 50% of human cancers (Kashani et al., 2018; Li et al., 2020; Merkle et al., 2017; Vogelstein et al., 2000).

To address the gap in knowledge of WDR5 function in ESCs with *p53* inactivation, we used *Wdr5*- and *p53*-null mESC lines with Dox-inducible WT and mutant forms of WDR5 to address H3K4 methylation-dependent and -independent gene regulation during mESC self-renewal and retinal neuroectoderm differentiation. First, we found that an H3K4 methylation-independent, WDR5-driven mechanism maintains *p53*-null mESC self-renewal and represses GCM-specific gene expression in *p53*-null POs under serum-free (SFEBq) conditions that induce retinal neuroectoderm fate. Second, we extended our previous findings (Li et al., 2020) and demonstrated that H3K4 methylation-dependent WDR5 promotes retinal neuroectoderm differentiation in *p53*-null POs. Finally, we revealed that acute inactivation of WDR5 leads to enhanced chromatin accessibility on most gene targets bound by MAX and WDR5. Thus, our work highlights the poorly understood, non-canonical role of MAX and WDR5 as two components of ncPRC1 for gene silencing/repression during mESC fate determination (Gao et al., 2012; Ogawa et al., 2002).

We found that self-renewal of *Wdr5* KO and DKO mESCs showed distinct requirements for WDR5-mediated H3K4 methylation. WDR5$^{S91K-Y191F}$ harbors defective H3K4 methylation activity but nevertheless supports

(E) Representative track views for gene region co-bound by MAX and WDR5 in WT POs and open chromatin accessibility observed in day 2 *Wdr5* KO POs.

(F) Western blot to detect MAX expression in day 2 WT and *Wdr5* KO POs.

(G) Overlapping of MAX-bound peaks lost in day 2 *Wdr5* KO and DKO POs.

(H) Representative track views for 5′ UTR of *Lsm4* gene, which is co-bound by MAX and WDR5 in day 2 WT POs.

(I) *Lsm4* mRNA expression at day 2 WT, *Wdr5* KO, and DKO POs determined by RNA-seq. N.S., no significant difference. **p $\leq$ 0.01 compared with WT controls. ****p $\leq$ 0.0001 compared with WT controls.

self-renewal of *Wdr5*- and *p53*-null mESCs, but not *Wdr5* KO mESCs. Thus, our data provide evidence that H3K4 methylation- or chromatin-independent mechanisms contribute to self-renewal of *p53*-null mESCs. An H3K4 methylation-independent function for WDR5 for regulating ciliogenesis and left-right patterning was recently reported in embryonic *Xenopus* models, with WT *p53* background (Kulkarni et al., 2018; Kulkarni and Khokha, 2018). To our knowledge, the current study is the first to demonstrate that H3K4 methylation-independent WDR5 activity regulates distinct functions in ESCs, which can be resolved from its H3K4 methylation-dependent features based on *p53* status. As S91 and Y191 occupy pharmacologically relevant positions in the WDR5 arginine pocket for design of WDR5-MLL1 inhibitors for epigenetic treatment of cancer (Grebien et al., 2015; Karatas et al., 2017; Patel et al., 2008b), we predict that *p53*-null cancer stem/progenitor cells might be less sensitive or resistant to WDR5 inhibitors that target S91 and Y191 sites. We observed that both *Wdr5* KO and DKO mESCs, which entirely lack WDR5, lose self-renewal capacity, albeit at different rates. Thus, additional strategies, such as PROTAC-mediated protein degradation, may be promising, future areas of exploration for WDR5 inhibition in *p53*-mutant cancers (Gadd et al., 2017).

During retinal neuroectoderm differentiation, we found that H3K4 methylation-dependent WDR5 functions promote cell fate determination in *p53*-null mESCs. An H3K4 methylation-dependent mechanism for WDR5-driven retinal neuroectoderm differentiation might be expected, since lineage-specifying loci are decorated by H3K4me3 and H3K27me3 bivalent chromatin in mESCs and developing retina (Bernstein et al., 2006; Popova et al., 2012; Rao et al., 2010). Roles for H3K4 methylation-dependent and -independent WDR5 functions, including WDR5 cytoplasmic roles, have been reported (Bailey et al., 2015; Kulkarni et al., 2018; Kulkarni and Khokha, 2018; Wang et al., 2010). In addition to WDR5, other H3K4 methyltransferase complex subunits, such as RbBP5 and Ash2L, also display dual nuclear and cytoplasmic distribution (Wang et al., 2017). Future studies, such as those employing mass spectrometry-based methods to identify specific WDR5-interacting partners in the cytoplasm of *p53*-null ESCs, will provide missing insights on how WDR5-driven cytoplasmic function may contribute to pluripotent stem cell fate determination.

A multifaceted protein, WDR5 is a subunit of the ncPRC1 complex and interplay of WDR5 with other ncPRC1 components to mediate transcriptional repression remains poorly understood (Endoh et al., 2017; Gao et al., 2012; Ogawa et al., 2002). Three subunits of ncPRC1, PCGF6, E2F6, and MAX, coordinately function as repressors for GCM-specific gene expression in mESCs (Endoh et al., 2017; Maeda et al., 2013; Stielow et al., 2018; Suzuki et al., 2016). *Pcgf6*-null mESCs maintain self-renewal while both *Max*-null or *Wdr5*-null KO mESCs lose clonogenicity. In this work, the functional significance of the interaction of MAX and WDR5 is demonstrated in GCM-specific gene repression. MAX is commonly studied vis-à-vis transcriptional regulation, as a transactivator dimerized with MYC (Blackwood and Eisenman, 1991). MYC also interacts with WDR5 via the same binding surface as RbBP5 but in a mutually exclusive manner (Thomas et al., 2015). Based on the fact that (1) GCM-related loci derepression is not found in *MYC* KO ESCs (Maeda et al., 2013) and that (2) WDR5-MYC interaction mutants $WDR5^{N225}$, $WDR5^{L240K}$, and $WDR5^{V268E}$ repress GCM-specific gene expression in DKO POs (data not shown), MYC interaction with MAX or WDR5 may not contribute significantly to GCM-related gene repression during differentiation of mESCs to retinal neuroectoderm. Future efforts using $Max^{flox/flox}$ and $Wdr5^{flox/flox}$ mESCs would allow us to test whether compound deletion of *Max* and *Wdr5* leads to synergistic de-repression of GCM-related gene induction or further promote PGCLC differentiation from mESCs. Such observations would provide deeper insights into the role of MAX-WDR5 interaction on repression of germ cell and meiosis-related loci.

Although the current study focuses on the chromatin-dependent function of WDR5 in current article, the role of p53 in DKO ESCs/POs deserves future study. During an unbiased loss-of-function CRISPR-Cas9 screening, loss of *p53* has been shown to promote PGCLC differentiation from mESCs (Hackett et al., 2018). Growth advantage of mESCs by *p53* deletion and upregulation of p53 target gene *Nanog* may account for enriched PGCLC differentiation (Lin et al., 2005; Murakami et al., 2016). However, Nanog expression was not upregulated in *Wdr5*- and *p53*-null POs. A possible mechanism for p53-mediated GCM-related gene repression in *Wdr5* KO POs may be through common targets such as *Dazl* and *Rhox5*, as those two GCM-related genes, regulated by DNA methylation (Jackson-Grusby et al., 2001), were both upregulated in *p53*-null cells and day 2 *Wdr5* KO POs (data not shown). Future studies that unravel mechanisms by which WDR5 exerts distinct chromatin-dependent and/or independent functions, vis-à-vis p53 activity, to determine pluripotent stem cell fate will be especially important. This is because a subset of the popularly used H1 (WA01) and H9 (WA09) hESC lines, and others, carry inactivating *TP53* mutations. These hESC lines are commonly used to model retinogenesis and cell transplantation in the laboratory and have been used in clinical trials (Hackett et al., 2018; Kashani et al., 2018; Phillips et al., 2012).

EXPERIMENTAL PROCEDURES

mESC maintenance, transfection, clonogenicity assay, and differentiation

Parental Rx:GFP (Eiraku et al., 2011) and independent *Wdr5* KO, *Wdr5*, and *p53* KO mESC lines (Li et al., 2020) were used for this study. mESCs were maintained in an undifferentiated status and differentiated to retinal neuroectoderm organoids as described previously (Assawachananont et al., 2014; Eiraku et al., 2011; Eiraku and Sasai, 2011; Li et al., 2020). InFusion kit (Takara) was used for WDR5 plasmid subcloning. A nucleofector device (Lonza) was used for mESCs transfection. A clonogenicity assay was used to confirm mESC self-renewal function as described previously (Ying et al., 2003).

ATAC-seq

Chromatin accessibility in undifferentiated mESCs and day 4 retinal neuroectoderm organoids were determined by ATAC-seq (Nextera DNA Library Prep Kit, Illumina).

ChIP-seq and CUT&RUN sequencing

In undifferentiated mESCs, WDR5 and H3K4me3 binding to DNA was determined by ChIP-seq and 1×10^8 cells were used. To assess WDR5 and MAX recruitment to DNA at day 2 retinal neuroectoderm differentiation, CUT&RUN assay was performed and 2×10^6 cells were used.

RNA-seq

Undifferentiated mESCs, day 4 retinal neuroectoderm organoids were harvested and RNA was extracted for bulk RNA-seq.

Data and code availability

ATAC-seq GEO under accession number GSE178551; ChIP-seq GEO under accession number GSE178552; CUT&RUN GEO under accession number GSE178554; RNA-seq GEO under accession number GSE178555.

SUPPLEMENTAL INFORMATION

Supplemental information can be found online at https://doi.org/10.1016/j.stemcr.2021.10.002.

AUTHOR CONTRIBUTIONS

Conceptualization, Q.L. and R.C.R.; methodology, Q.L., Y.H., J.X., F.M., B.Z., L.S., B.W.B., M.A., J.L., Y.D., and R.C.R.; software and computational analysis, Y.H. and F.M; investigation, Q.L., Y.H., F.M., J.X., B.Z., L.S., J.L., and Y.D.; resources, J.L., Y.D., and R.C.R.; writing – original draft, Q.L. and R.C.R.; writing – review & editing, Q.L., Y.H., J.L., Y.D., and R.C.R.; supervision, R.C.R.; funding acquisition, R.C.R.

CONFLICT OF INTERESTS

The authors declare no competing interests.

ACKNOWLEDGMENTS

This research was supported by the National Eye Institute (K08EY026654 and R01EY030989, to R.C.R), the National Cancer Institute (P30CA046592, to the University of Michigan Comprehensive Cancer Center), the National Institute of General Medical Sciences (B.W.B. supported by T32GM141840) and Research to Prevent Blindness (to the University of Michigan Kellogg Eye Center and R.C.R.). R.C.R. received funding from the Beatrice & Reymont Paul Foundation , March Hoops to Beat Blindness , the Taubman Institute , the Leonard G. Miller Endowed Professorship and Ophthalmic Research Fund at the Kellogg Eye Center , and the Grossman , Elaine Sandman , Marek and Maria Spatz (endowed), Greenspon , Dunn , Avers , Boustikakis , Sweiden , and Terauchi research funds.

Received: September 15, 2020
Revised: October 3, 2021
Accepted: October 4, 2021
Published: October 28, 2021

REFERENCES

Ang, Y.S., Tsai, S.Y., Lee, D.F., Monk, J., Su, J., Ratnakumar, K., Ding, J., Ge, Y., Darr, H., Chang, B., et al. (2011). Wdr5 mediates self-renewal and reprogramming via the embryonic stem cell core transcriptional network. Cell *145*, 183–197.

Assawachananont, J., Mandai, M., Okamoto, S., Yamada, C., Eiraku, M., Yonemura, S., Sasai, Y., and Takahashi, M. (2014). Transplantation of embryonic and induced pluripotent stem cell-derived 3D retinal sheets into retinal degenerative mice. Stem Cell Reports *2*, 662–674.

Bailey, J.K., Fields, A.T., Cheng, K., Lee, A., Wagenaar, E., Lagrois, R., Schmidt, B., Xia, B., and Ma, D. (2015). WD repeat-containing protein 5 (WDR5) localizes to the midbody and regulates abscission. J. Biol. Chem. *290*, 8987–9001.

Bernstein, B.E., Mikkelsen, T.S., Xie, X., Kamal, M., Huebert, D.J., Cuff, J., Fry, B., Meissner, A., Wernig, M., Plath, K., et al. (2006). A bivalent chromatin structure marks key developmental genes in embryonic stem cells. Cell *125*, 315–326.

Blackwood, E.M., and Eisenman, R.N. (1991). Max: a helix-loop-helix zipper protein that forms a sequence-specific DNA-binding complex with Myc. Science *251*, 1211–1217.

Blazevits, O., Bolshette, N., Vecchio, D., Guijarro, A., Croci, O., Campaner, S., and Grimaldi, B. (2020). MYC-associated factor MAX is a regulator of the circadian clock. Int. J. Mol. Sci. *21*, 2294.

Dou, Y., Milne, T.A., Ruthenburg, A.J., Lee, S., Lee, J.W., Verdine, G.L., Allis, C.D., and Roeder, R.G. (2006). Regulation of MLL1 H3K4 methyltransferase activity by its core components. Nat. Struct. Mol. Biol. *13*, 713–719.

Dou, Y., Milne, T.A., Tackett, A.J., Smith, E.R., Fukuda, A., Wysocka, J., Allis, C.D., Chait, B.T., Hess, J.L., and Roeder, R.G. (2005). Physical association and coordinate function of the H3 K4 methyltransferase MLL1 and the H4 K16 acetyltransferase MOF. Cell *121*, 873–885.

Eiraku, M., and Sasai, Y. (2011). Mouse embryonic stem cell culture for generation of three-dimensional retinal and cortical tissues. Nat. Protoc. *7*, 69–79.

Eiraku, M., Takata, N., Ishibashi, H., Kawada, M., Sakakura, E., Okuda, S., Sekiguchi, K., Adachi, T., and Sasai, Y. (2011). Self-organizing optic-cup morphogenesis in three-dimensional culture. Nature *472*, 51–56.

Endoh, M., Endo, T.A., Shinga, J., Hayashi, K., Farcas, A., Ma, K.W., Ito, S., Sharif, J., Endoh, T., Onaga, N., et al. (2017). PCGF6-PRC1 suppresses premature differentiation of mouse embryonic stem cells by regulating germ cell-related genes. eLife *6*, e21064.

Gadd, M.S., Testa, A., Lucas, X., Chan, K.H., Chen, W., Lamont, D.J., Zengerle, M., and Ciulli, A. (2017). Structural basis of PROTAC cooperative recognition for selective protein degradation. Nat. Chem. Biol. *13*, 514–521.

Gan, Q., Thiebaud, P., Theze, N., Jin, L., Xu, G., Grant, P., and Owens, G.K. (2011). WD repeat-containing protein 5, a ubiquitously expressed histone methyltransferase adaptor protein, regulates smooth muscle cell-selective gene activation through interaction with pituitary homeobox 2. J. Biol. Chem. *286*, 21853–21864.

Gao, Z., Zhang, J., Bonasio, R., Strino, F., Sawai, A., Parisi, F., Kluger, Y., and Reinberg, D. (2012). PCGF homologs, CBX proteins, and RYBP define functionally distinct PRC1 family complexes. Mol. Cell *45*, 344–356.

Giaccia, A.J., and Kastan, M.B. (1998). The complexity of p53 modulation: emerging patterns from divergent signals. Genes Dev. *12*, 2973–2983.

Grebien, F., Vedadi, M., Getlik, M., Giambruno, R., Grover, A., Avellino, R., Skucha, A., Vittori, S., Kuznetsova, E., Smil, D., et al. (2015). Pharmacological targeting of the Wdr5-MLL interaction in C/EBPalpha N-terminal leukemia. Nat. Chem. Biol. *11*, 571–578.

Greenbaum, M.P., Ma, L., and Matzuk, M.M. (2007). Conversion of midbodies into germ cell intercellular bridges. Dev. Biol. *305*, 389–396.

Hackett, J.A., Huang, Y., Gunesdogan, U., Gretarsson, K.A., Kobayashi, T., and Surani, M.A. (2018). Tracing the transitions from pluripotency to germ cell fate with CRISPR screening. Nat. Commun. *9*, 4292.

Haupt, Y., Maya, R., Kazaz, A., and Oren, M. (1997). Mdm2 promotes the rapid degradation of p53. Nature *387*, 296–299.

Hayashi, K., Ohta, H., Kurimoto, K., Aramaki, S., and Saitou, M. (2011). Reconstitution of the mouse germ cell specification pathway in culture by pluripotent stem cells. Cell *146*, 519–532.

Jackson-Grusby, L., Beard, C., Possemato, R., Tudor, M., Fambrough, D., Csankovszki, G., Dausman, J., Lee, P., Wilson, C., Lander, E., et al. (2001). Loss of genomic methylation causes p53-dependent apoptosis and epigenetic deregulation. Nat. Genet. *27*, 31–39.

Karatas, H., Li, Y., Liu, L., Ji, J., Lee, S., Chen, Y., Yang, J., Huang, L., Bernard, D., Xu, J., et al. (2017). Discovery of a highly potent, cell-permeable macrocyclic peptidomimetic (MM-589) targeting the WD repeat domain 5 protein (WDR5)-mixed lineage leukemia (MLL) protein-protein interaction. J. Med. Chem. *60*, 4818–4839.

Kashani, A.H., Lebkowski, J.S., Rahhal, F.M., Avery, R.L., Salehi-Had, H., Dang, W., Lin, C.M., Mitra, D., Zhu, D., Thomas, B.B., et al. (2018). A bioengineered retinal pigment epithelial monolayer for advanced, dry age-related macular degeneration. Sci. Transl. Med. *10*, eaao4097.

Kim, D.K., Cha, Y., Ahn, H.J., Kim, G., and Park, K.S. (2014a). Lefty1 and lefty2 control the balance between self-renewal and pluripotent differentiation of mouse embryonic stem cells. Stem Cells Dev. *23*, 457–466.

Kim, J.Y., Banerjee, T., Vinckevicius, A., Luo, Q., Parker, J.B., Baker, M.R., Radhakrishnan, I., Wei, J.J., Barish, G.D., and Chakravarti, D. (2014b). A role for WDR5 in integrating threonine 11 phosphorylation to lysine 4 methylation on histone H3 during androgen signaling and in prostate cancer. Mol. Cell *54*, 613–625.

Kulkarni, S.S., Griffin, J.N., Date, P.P., Liem, K.F., Jr., and Khokha, M.K. (2018). WDR5 stabilizes actin architecture to promote multiciliated cell formation. Dev. Cell *46*, 595–610 e593.

Kulkarni, S.S., and Khokha, M.K. (2018). WDR5 regulates left-right patterning via chromatin-dependent and -independent functions. Development *145*, dev159889.

Li, Q., Mao, F., Zhou, B., Huang, Y., Zou, Z., denDekker, A.D., Xu, J., Hou, S., Liu, J., Dou, Y., et al. (2020). p53 integrates temporal WDR5 inputs during neuroectoderm and mesoderm differentiation of mouse embryonic stem cells. Cell Rep. *30*, 465–480 e466.

Li, X., Li, L., Pandey, R., Byun, J.S., Gardner, K., Qin, Z., and Dou, Y. (2012). The histone acetyltransferase MOF is a key regulator of the embryonic stem cell core transcriptional network. Cell Stem Cell *11*, 163–178.

Lin, T., Chao, C., Saito, S., Mazur, S.J., Murphy, M.E., Appella, E., and Xu, Y. (2005). p53 induces differentiation of mouse embryonic stem cells by suppressing Nanog expression. Nat. Cell Biol. *7*, 165–171.

Liu, P., Dou, X., Liu, C., Wang, L., Xing, C., Peng, G., Chen, J., Yu, F., Qiao, Y., Song, L., et al. (2015). Histone deacetylation promotes mouse neural induction by restricting nodal-dependent mesendoderm fate. Nat. Commun. *6*, 6830.

Maeda, I., Okamura, D., Tokitake, Y., Ikeda, M., Kawaguchi, H., Mise, N., Abe, K., Noce, T., Okuda, A., and Matsui, Y. (2013). Max is a repressor of germ cell-related gene expression in mouse embryonic stem cells. Nat. Commun. *4*, 1754.

Marion, R.M., Strati, K., Li, H., Murga, M., Blanco, R., Ortega, S., Fernandez-Capetillo, O., Serrano, M., and Blasco, M.A. (2009). A p53-mediated DNA damage response limits reprogramming to ensure iPS cell genomic integrity. Nature *460*, 1149–1153.

Martinerie, L., Manterola, M., Chung, S.S., Panigrahi, S.K., Weisbach, M., Vasileva, A., Geng, Y., Sicinski, P., and Wolgemuth, D.J. (2014). Mammalian E-type cyclins control chromosome pairing, telomere stability and CDK2 localization in male meiosis. PLoS Genet. *10*, e1004165.

Meers, M.P., Bryson, T.D., Henikoff, J.G., and Henikoff, S. (2019a). Improved CUT&RUN chromatin profiling tools. eLife *8*, e46314.

Meers, M.P., Tenenbaum, D., and Henikoff, S. (2019b). Peak calling by sparse enrichment analysis for CUT&RUN chromatin profiling. Epigenetics Chromatin *12*, 42.

Merkle, F.T., Ghosh, S., Kamitaki, N., Mitchell, J., Avior, Y., Mello, C., Kashin, S., Mekhoubad, S., Ilic, D., Charlton, M., et al. (2017). Human pluripotent stem cells recurrently acquire and expand dominant negative P53 mutations. Nature *545*, 229–233.

Murakami, K., Gunesdogan, U., Zylicz, J.J., Tang, W.W.C., Sengupta, R., Kobayashi, T., Kim, S., Butler, R., Dietmann, S., and Surani, M.A. (2016). NANOG alone induces germ cells in primed epiblast in vitro by activation of enhancers. Nature *529*, 403–407.

Nady, N., Gupta, A., Ma, Z., Swigut, T., Koide, A., Koide, S., and Wysocka, J. (2015). ETO family protein Mtgr1 mediates Prdm14 functions in stem cell maintenance and primordial germ cell formation. eLife *4*, e10150.

Niu, C., Wang, S., Guo, J., Wei, X., Jia, M., Chen, Z., Gong, W., Qin, Y., Wang, X., Zhi, X., et al. (2021). BACH1 recruits NANOG and histone H3 lysine 4 methyltransferase MLL/SET1 complexes to regulate enhancer-promoter activity and maintains pluripotency. Nucleic Acids Res. *49*, 1972–1986.

Ogawa, H., Ishiguro, K., Gaubatz, S., Livingston, D.M., and Nakatani, Y. (2002). A complex with chromatin modifiers that occupies E2F- and Myc-responsive genes in G0 cells. Science *296*, 1132–1136.

Patel, A., Dharmarajan, V., and Cosgrove, M.S. (2008a). Structure of WDR5 bound to mixed lineage leukemia protein-1 peptide. J. Biol. Chem. *283*, 32158–32161.

Patel, A., Vought, V.E., Dharmarajan, V., and Cosgrove, M.S. (2008b). A conserved arginine-containing motif crucial for the assembly and enzymatic activity of the mixed lineage leukemia protein-1 core complex. J. Biol. Chem. *283*, 32162–32175.

Phillips, M.J., Wallace, K.A., Dickerson, S.J., Miller, M.J., Verhoeven, A.D., Martin, J.M., Wright, L.S., Shen, W., Capowski, E.E., Percin, E.F., et al. (2012). Blood-derived human iPS cells generate optic vesicle-like structures with the capacity to form retinal laminae and develop synapses. Invest. Ophthalmol. Vis. Sci. *53*, 2007–2019.

Popova, E.Y., Xu, X., DeWan, A.T., Salzberg, A.C., Berg, A., Hoh, J., Zhang, S.S., and Barnstable, C.J. (2012). Stage and gene specific signatures defined by histones H3K4me2 and H3K27me3 accompany mammalian retina maturation in vivo. PLoS One *7*, e46867.

Rao, R.C., and Dou, Y. (2015). Hijacked in cancer: the KMT2 (MLL) family of methyltransferases. Nat. Rev. Cancer *15*, 334–346.

Rao, R.C., Tchedre, K.T., Malik, M.T., Coleman, N., Fang, Y., Marquez, V.E., and Chen, D.F. (2010). Dynamic patterns of histone lysine methylation in the developing retina. Invest. Ophthalmol. Vis. Sci. *51*, 6784–6792.

Sabapathy, K., Klemm, M., Jaenisch, R., and Wagner, E.F. (1997). Regulation of ES cell differentiation by functional and conformational modulation of p53. EMBO J. *16*, 6217–6229.

Sammons, M.A., Zhu, J., Drake, A.M., and Berger, S.L. (2015). TP53 engagement with the genome occurs in distinct local chromatin environments via pioneer factor activity. Genome Res. *25*, 179–188.

Schapira, M., Tyers, M., Torrent, M., and Arrowsmith, C.H. (2017). WD40 repeat domain proteins: a novel target class? Nat. Rev. Drug Discov. *16*, 773–786.

Shyh-Chang, N., and Daley, G.Q. (2013). Lin28: primal regulator of growth and metabolism in stem cells. Cell Stem Cell *12*, 395–406.

Stielow, B., Finkernagel, F., Stiewe, T., Nist, A., and Suske, G. (2018). MGA, L3MBTL2 and E2F6 determine genomic binding of the non-canonical Polycomb repressive complex PRC1.6. PLoS Genet. *14*, e1007193.

Suzuki, A., Hirasaki, M., Hishida, T., Wu, J., Okamura, D., Ueda, A., Nishimoto, M., Nakachi, Y., Mizuno, Y., Okazaki, Y., et al. (2016). Loss of MAX results in meiotic entry in mouse embryonic and germline stem cells. Nat. Commun. *7*, 11056.

Thomas, L.R., Wang, Q., Grieb, B.C., Phan, J., Foshage, A.M., Sun, Q., Olejniczak, E.T., Clark, T., Dey, S., Lorey, S., et al. (2015). Interaction with WDR5 promotes target gene recognition and tumorigenesis by MYC. Mol. Cell *58*, 440–452.

Velasco, G., Hube, F., Rollin, J., Neuillet, D., Philippe, C., Bouzinba-Segard, H., Galvani, A., Viegas-Pequignot, E., and Francastel, C. (2010). Dnmt3b recruitment through E2F6 transcriptional repressor mediates germ-line gene silencing in murine somatic tissues. Proc. Natl. Acad. Sci. U S A *107*, 9281–9286.

Vogelstein, B., Lane, D., and Levine, A.J. (2000). Surfing the p53 network. Nature *408*, 307–310.

Wang, L., Collings, C.K., Zhao, Z., Cozzolino, K.A., Ma, Q., Liang, K., Marshall, S.A., Sze, C.C., Hashizume, R., Savas, J.N., et al. (2017). A cytoplasmic COMPASS is necessary for cell survival and triple-negative breast cancer pathogenesis by regulating metabolism. Genes Dev. *31*, 2056–2066.

Wang, Y.Y., Liu, L.J., Zhong, B., Liu, T.T., Li, Y., Yang, Y., Ran, Y., Li, S., Tien, P., and Shu, H.B. (2010). WDR5 is essential for assembly of the VISA-associated signaling complex and virus-triggered IRF3 and NF-kappaB activation. Proc. Natl. Acad. Sci. U S A *107*, 815–820.

Wu, J., Huang, B., Chen, H., Yin, Q., Liu, Y., Xiang, Y., Zhang, B., Liu, B., Wang, Q., Xia, W., et al. (2016). The landscape of accessible chromatin in mammalian preimplantation embryos. Nature *534*, 652–657.

Wysocka, J., Swigut, T., Milne, T.A., Dou, Y., Zhang, X., Burlingame, A.L., Roeder, R.G., Brivanlou, A.H., and Allis, C.D. (2005). WDR5 associates with histone H3 methylated at K4 and is essential for H3 K4 methylation and vertebrate development. Cell *121*, 859–872.

Xue, H., Yao, T., Cao, M., Zhu, G., Li, Y., Yuan, G., Chen, Y., Lei, M., and Huang, J. (2019). Structural basis of nucleosome recognition and modification by MLL methyltransferases. Nature *573*, 445–449.

Ying, Q.L., Nichols, J., Chambers, I., and Smith, A. (2003). BMP induction of Id proteins suppresses differentiation and sustains embryonic stem cell self-renewal in collaboration with STAT3. Cell *115*, 281–292.

Yue, F., Cheng, Y., Breschi, A., Vierstra, J., Wu, W., Ryba, T., Sandstrom, R., Ma, Z., Davis, C., Pope, B.D., et al. (2014). A comparative encyclopedia of DNA elements in the mouse genome. Nature *515*, 355–364.

Zagore, L.L., Sweet, T.J., Hannigan, M.M., Weyn-Vanhentenryck, S.M., Jobava, R., Hatzoglou, M., Zhang, C., and Licatalosi, D.D. (2018). DAZL regulates germ cell survival through a network of PolyA-proximal mRNA interactions. Cell Rep. *25*, 1225–1240 e1226.

Zhu, J., Sammons, M.A., Donahue, G., Dou, Z., Vedadi, M., Getlik, M., Barsyte-Lovejoy, D., Al-awar, R., Katona, B.W., Shilatifard, A., et al. (2015). Gain-of-function p53 mutants co-opt chromatin pathways to drive cancer growth. Nature *525*, 206–211.